THE STRUCTURE OF CLOSE BINARIES IN TWO DIMENSIONS

R. G. DEUPREE AND A. I. KARAKAS

Institute for Computational Astrophysics, Department of Astronomy and Physics, Saint Mary's University,
Halifax, NS B3H 3C3, Canada; bdeupree@ap.smu.ca, akarakas@ap.smu.ca

ABSTRACT

The structure and evolution of close binary stars has been studied using the two-dimensional stellar structure algorithm developed by Deupree. We have calculated a series of solar composition stellar evolution sequences of binary models in which the mass of the two-dimensional model is 8 $M_\odot$ with a point-mass 5 $M_\odot$ companion. We have also studied the structure of the companion in two dimensions by considering the zero-age main sequence (ZAMS) structure of a 5 $M_\odot$ model with an 8 $M_\odot$ point-mass companion. This result suggests that treating the 5 $M_\odot$ star as a point source for the 8 $M_\odot$ evolution is reasonable. In all cases, the binary orbit was assumed to be circular and corotating with the rotation rate of the stars. We considered binary models with three different initial separations, $a = 10,\ 14,$ and 20 $R_\odot$. These models were evolved through central hydrogen burning or until the more massive star expanded to fill its critical potential surface or Roche lobe. The model with a separation of 20 $R_\odot$ will be expected to go through case B–type mass transfer during the shell H-burning phase. The 14 $R_\odot$ model is expected to go through mass transfer much earlier, near the middle of core hydrogen burning, and the 10 $R_\odot$ model is very close to this situation at the ZAMS. The calculations show that evolution of the deep interior quantities is only slightly modified from those of single-star evolution. Describing the model surface as a Roche equipotential is also satisfactory until very close to the time of Roche lobe overflow, when the self-gravity of the model about to lose mass develops a noticeable aspherical component and the surface timescale becomes sufficiently short, so that it is conceivable that the actual surface is not an equipotential.

Subject headings: binaries: close — stars: interiors

1. INTRODUCTION

Much progress has been made in understanding the structure and evolution of single stars. This is because we assume that the stars are spherically symmetric and in, or close to, hydrostatic equilibrium for most of their evolution, allowing the use of one-dimensional models. Observations have shown that there are places where these assumptions do not hold, for example, in rapidly rotating main-sequence stars such as the Be star Achernar (Domiciano de Souza et al. 2003; Jackson et al. 2004; Lovekin et al. 2004). Binary (or multiple) star evolution, on the other hand, is far more complex because of the possibility of the two components interacting, which depends on the mass of the stars and the orbital parameters of the system. However, it is essential that the evolution of multiple stellar systems be studied, given that most stars in the solar neighborhood are observed to be in such systems. Many of the interacting stars are observed to be undergoing mass transfer via Roche lobe overflow (RLOF), which results in a veritable zoo of stellar subtypes, including the W Ursae Majoris contact binaries (Li et al. 2004 and references therein) and the Algol-type binaries (Nelson & Eggleton 2001), which are formed by mass transfer on or near the main sequence. Other subtypes, such as cataclysmic variables, novae, and symbiotics (Iben & Tutukov 1996), X-ray binaries (Verbunt 1993), and black hole X-ray novae (for example, McClintock et al. 2001) are all formed through one or more mass transfer events when the stars are in the final stages of stellar evolution. The recent high-quality X-ray observations have been providing important links between some of these subtypes, including classical and recurrent novae experiencing X-ray emission, symbiotics, and cataclysmic variables (Podsiadlowski et al. 2002; Wheatley et al. 2003). Millisecond pulsars are also an important class of objects that are formed when mass is transferred from a companion onto an old neutron

star, resulting in the spin-up of the neutron star (Phinney & Kulkarni 1994). Stellar nucleosynthesis and Galactic chemical evolution also depend on the interactions between binary stars to produce explosive events such as classical novae or Type Ia supernovae, where asymmetric effects play an important role (Thielemann et al. 2004; Yoon & Langer 2004). Recent work suggests that the presence of a binary companion may also be important for Type II supernova explosions (Podsiadlowski et al. 2004).

The pioneering studies by Kippenhahn & Weigert (1967), Paczynski (1966, 1967, 1971), and Paczynski & Ziólkowski (1967) set the stage for much of the work that followed on close binary evolution, which by definition involves systems in which the two stars are close enough to allow at least one phase of mass transfer via RLOF. These early studies focused on upper main-sequence stars that were evolved through either classical case A mass transfer, which takes place during the main sequence, or case B mass transfer, which takes place after the exhaustion of central hydrogen (Kippenhahn & Weigert 1967). While the input physics and the stellar models have undergone significant improvements in recent years, the assumptions made when calculating binary evolution remain essentially the same as those used in these early studies (for example, Nelson & Eggleton 2001): that a star in a binary system is treated as spherically symmetric, even if it fills its Roche lobe; that the mass transfer from a star that overfills its Roche lobe is treated as spherically symmetric; that the matter that leaves the mass-losing star is accreted in a spherically symmetric manner on the surface of the mass-gaining star; that the orbit is circular (although see Regős et al. [2005] for a relaxation of this assumption); that the star is assumed to be in hydrostatic equilibrium; that there is a critical radius R_L such that mass exchange takes place when $R \geq R_L$; and that the radius of a star is always equal to or less than R_L. The total mass of the system and

the angular orbital momentum are also conserved during the evolution. In this study, we are concerned with the first assumption; i.e., how valid is the assumption of spherical symmetry up to the beginning of mass transfer? The key points of the one-dimensional approach are that the interior is unaffected by the presence of the companion, while the surface is defined as a Roche potential surface for two gravitational point sources.

While the proper way to treat this problem is in three dimensions, we can adequately describe the problem in two dimensions if we assume that the orbit is circular and corotating with the spins of the two stars. We have used the two-dimensional structure algorithm developed by Deupree (1990, 1995) to study the structure and evolution of intermediate-mass solar composition stars with a point-mass companion. The models we consider are of a similar mass and composition studied by Paczynski in his early series of papers on the evolution of close binary evolution (Paczynski 1966, 1967; Paczynski & Ziólkowski 1967), which assumed a mass of 8 $M_\odot$ for the more massive component (hereafter the primary) and 5.3 $M_\odot$ for the least massive component (hereafter the secondary). The aim of this paper is to study the evolution and structure of an 8 $M_\odot$ primary with a 5 $M_\odot$ point-mass companion, from the ZAMS through to the end of central H burning, or to the point where mass transfer is expected to begin. We investigate varying the separation between the stars, from 10 to 20 $R_\odot$ (corresponding to periods of 1.01–2.86 days, respectively). The results from these stellar models are examined to see if they satisfy the constraints used in studies of close binary evolution; namely, does the primary star remain in, or close to, spherical symmetry prior to RLOF? We have also studied the ZAMS structure of a 5 $M_\odot$ model with an 8 $M_\odot$ point source to see if the assumption of treating the secondary star as a point-mass source is reasonable.

The paper is organized as follows. The numerical method is presented in § 2 along with details of the stellar models calculated. In § 3 we present our results, and we finish with a discussion and some conclusions in § 4.

2. MODELS

The stellar models were calculated with the two-dimensional stellar structure, evolution, and hydrodynamics code developed by Deupree (1990, 1995). The algorithm uses a two-dimensional finite-difference approach to solve the appropriate equations via a fully implicit Henyey (Henyey et al. 1964) technique. More strictly speaking, the calculations are 2.5-dimensional because the azimuthal velocity is calculated even though azimuthal symmetry is imposed. The independent variables are the fractional surface radius, the spherical polar coordinate (θ), and time. The equations to be solved simultaneously in the implicit formulation are the conservation laws for mass, three components of momentum, energy, and hydrogen abundance, along with Poisson's equation. The dependent variables are the temperature, density, three components of velocity, hydrogen-mass fraction, and the gravitational potential. The unknown surface radius is determined from the equation that the integral of the density distribution over the volume equals the total mass. The usual subsidiary relations are satisfied with the composite hydrogen-burning nuclear energy generation rates (Fowler et al. 1967), the OPAL equation of state (Rogers et al. 1996), and OPAL radiative opacity (Iglesias & Rogers 1996). The latter two are included as tables, with values and numerical derivatives brought into the Jacobian needed for the Henyey iteration scheme as required.

Because the independent variables are not Lagrangian variables, we must calculate the velocities to determine how the material moves with respect to the coordinate system. Thus, we must re-

tain all advective and time-dependent terms in the equations. Unlike our approach to rotating stars (Deupree 1990; Lovekin et al. 2004), in which the calculations are performed in the inertial frame, here the calculations are performed in a coordinate system that is rotating at a constant rate. The rotation rate is given by the orbital period of the two bodies tidally locked in a circular orbit. This rate is not allowed to change in the calculations presented here, which covers the time from the ZAMS up to just before RLOF, which is justified since no mass is allowed to be lost from the system (via a stellar wind, for example), and hence the angular momentum is constant.

We must prescribe the shape of the surface. For rotating stars this is done by assuming the centrifugal acceleration can be described by a potential, even when this may not be true. In the binary star calculations presented here, we force the surface to be an equipotential whose three components are the self-gravity of the model being calculated, the point-source gravitational potential of the companion, and the potential arising from the centrifugal acceleration of the rotating coordinate system. The surface boundary condition for the self-gravitational potential is calculated for each angle on the surface of a sphere just exterior to the largest radius of the model. This condition is given by a weighted integral of the density distribution over the volume of the model, and these integrals are included as part of the Henyey iteration scheme.

The convective core is taken to be adiabatic. No convective overshooting is included in these calculations. There are no convective envelopes in the models computed here, so no recourse to a nonadiabatic convection theory is required. The surface temperature is taken to be the effective temperature divided by the fourth root of 2, and the radiation of the companion on the surface of the primary is neglected, the implications of which are discussed further in § 4.

The geometry of the calculations is that the model is symmetric about the axis defined by the centers of the two stars. In the star we are modeling, we take the value of the spherical polar coordinate, θ, to be $0°$ in the direction opposite the companion and $180°$ in the direction toward the companion. Thus, our model is a prolate spheroid. In addition, the rotation axis is at $\theta = 90°$ at the azimuthal angle, so that the rotation axis is perpendicular to the orbital plane. The rotation imposes symmetry about the rotation axis (which is perpendicular to the line between the stellar centers), so that the model really should be an ellipsoid instead of a spheroid. However, even at close separations of the two stars, the centrifugal acceleration is sufficiently small in comparison with the gravitational acceleration of the companion that a spheroidal shape is not a bad approximation, and that is adopted here.

We address three specific configurations. The primary is an 8 $M_\odot$ model, and the secondary has 5 $M_\odot$. We only consider evolution prior to mass transfer, so these designations are unambiguous. The three cases we consider are separations between the stellar centers of 10, 14, and 20 $R_\odot$. The primary in the first case fills its Roche lobe very soon after the ZAMS, and in the third case fills its Roche lobe relatively early in hydrogen shell burning. The filling of the Roche lobe by the primary in the second case occurs when nearly half of the hydrogen in the core has been burned. We also compare the evolution of these primaries with that of a spherical single star performed with the same radial and angular zoning. In these models we have 450 radial zones for the longest radius and 20 angular zones. Most of our calculations focus on the evolution of the primary, but we also examine the ZAMS model of the secondary (in the presence of a point-source potential with the primary's mass) to obtain some estimate as to how realistic a point-source potential for the secondary in the primary evolution calculations might be.

3. RESULTS

The assessment of the applicability of the one-dimensional approach has two components: the interior evolution and the surface characteristics. To this end, we have evolved three 8 $M_\odot$ models from the ZAMS until just before Roche overflow begins. We stop the calculations at this point because the two-dimensional surface boundary conditions would no longer be adequate once the component being modeled begins to lose mass to the other binary member.

We first examine the central conditions of the model with the greatest separation in Figure 1, a plot of the central temperature versus the central density. The differences in the central temperature for a given central density between the binary and the single-star models for this separation are about 0.3%, a number that is reasonably constant throughout the entire main-sequence evolution. The difference in percentage terms is approximately double this amount for the intermediate separation case and about 1.8% for the smallest separation. Because this last case is already very close to RLOF on the ZAMS, it is clear that the percentage cannot be much higher than this.

The mass of the convective core is plotted as a function of the central hydrogen abundance in Figure 2 for the intermediate separation case. Here we see that this is unaffected by the presence of the binary companion as well. However, it is true that the shape of the convective core boundary is not spherical but rather is elongated slightly in the direction of the binary companion. The elongation is only a fraction of a radial zone in the largest separation case, a bit more than a zone in the intermediate separation, and about two zones in the small separation case. At the convective core boundary location, the zone size is about 0.004 of the surface radius, and a radial zone contains about 0.1 $M_\odot$ when integrated over all angles. From these considerations it appears that the interior quantities are not much affected by the presence of the companion.

We now turn to the surface configuration. We frame our discussion in terms of the elongation of the model. The elongation is defined as the ratio of the surface radius in the direction opposite the binary companion to the surface radius in the direction of the binary companion. When the ratio is above about 0.9, we find that the Roche equipotential fits the surface shape as accu-
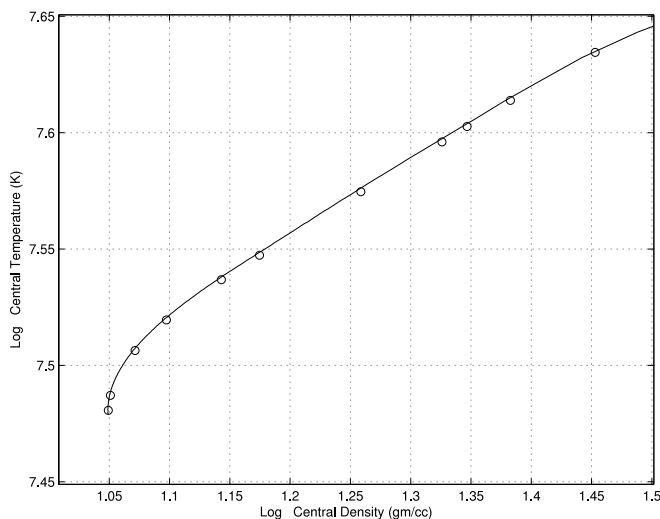
Fig. 2.—Plot of the mass of the convective core vs. the central hydrogen-mass fraction for the evolution of a single 8 $M_\odot$ model (*solid line*) and an 8 $M_\odot$ model with a 5 $M_\odot$ companion with a separation between the centers of the models of 14 $R_\odot$ (*circles*). The mass of the convective core is essentially unaffected by the presence of a companion, even though the shape of the convective core in the binary case is not perfectly spherical.

rately as we can measure with our discrete zoning (approximately 0.4%). As the elongation approaches 0.8, the two shapes are slightly different, mostly in the direction between the two components of the binary system. This is shown in Figure 3, a plot of the surface shape for the largest separation model just before the gravitational contraction phase begins. The difference in surface shape between the ROTORC and Roche models becomes more significant as RLOF is approached. A comparison for a model very close to RLOF (elongation of about 0.69) for the

Fig. 1.—Central temperature vs. the central density for the evolution of a single 8 $M_\odot$ model (*solid line*) and an 8 $M_\odot$ model with a 5 $M_\odot$ companion with a separation between the centers of the models of 20 $R_\odot$ (*circles*). The difference in the central densities for a given central temperature is about 0.3% and is nearly constant throughout the solution.
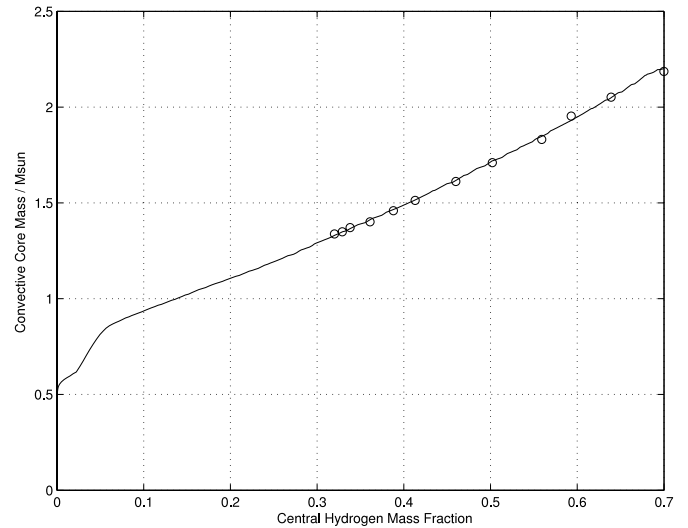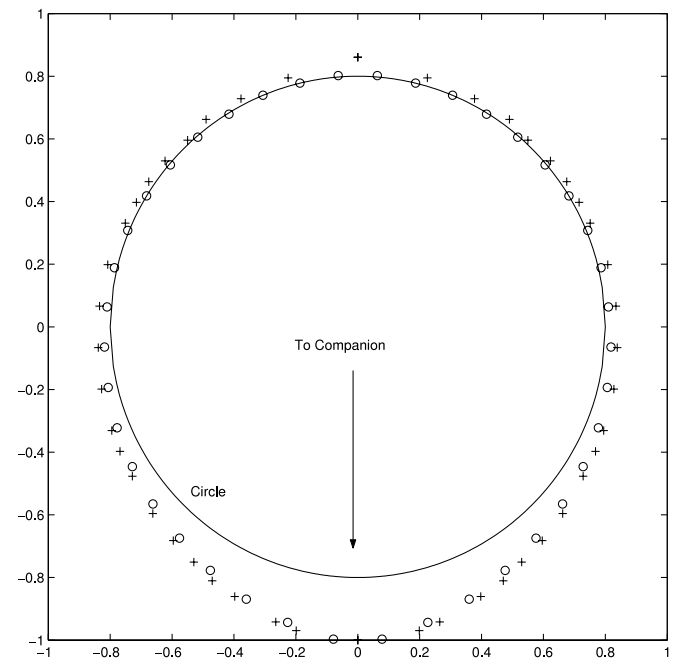
Fig. 3.—Comparison of the surface shape of the 8 $M_\odot$ primary with a 5 $M_\odot$ secondary, as determined by the two-dimensional stellar evolution code (*circles*) and the Roche potential surface (*plus signs*). The location of the secondary is below the bottom of the graph centered at a y-coordinate of −2.54. The solid curve is a circle to help highlight the departures from a spherical surface. The two surfaces are quite close, except near the line between the centers.
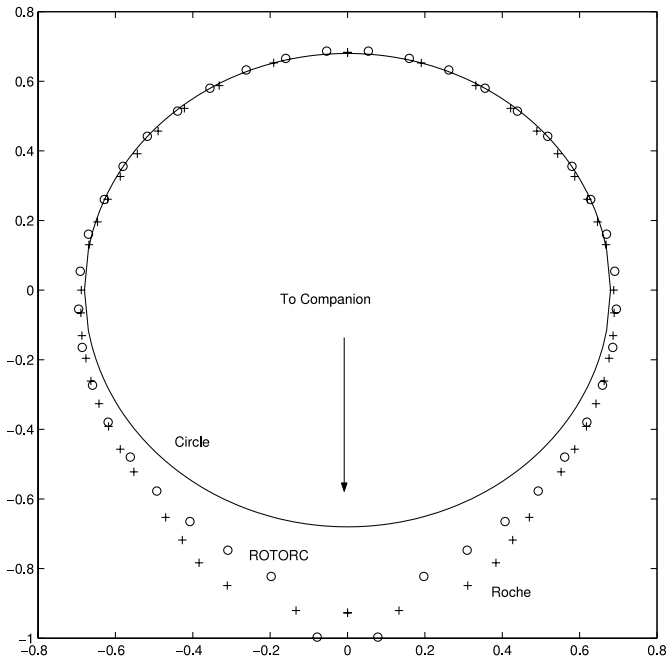
Fig. 4.—Comparison of the surface shape of the 8 $M_\odot$ primary with a 5 $M_\odot$ secondary, as determined by the two-dimensional stellar evolution code (*circles*) and the Roche potential surface (*plus signs*) for the intermediate separation case. The location of the secondary is below the bottom of the graph centered at a y-coordinate of -1.97. This model is very close to RLOF. The solid curve is a circle to highlight the departures from a spherical surface. Note that the Roche potential surface and the two-dimensional stellar evolution code surfaces differ close to the line between the two models. Part of this is just the sensitivity to the shape of the Roche potential surface to the exact value of the contour as RLOF is approached.

intermediate separation case is shown in Figure 4. There is clearly a difference in the two potentials in the direction between the two binary components. To be fair, the Roche potential contours are changing quite rapidly here, in the direction of looking more like the ROTORC contours for slightly larger fractional radii.

Clearly, one factor in the differing potentials is the possibility that the self-gravity of the primary at the model surface is not that given by the point-source potential. The self-gravitational potential of the primary on a spherical surface whose radius is given by the largest surface radius in the model is shown in Figure 5. Clearly, the magnitude of the potential is largest in the direction between the two components, and the amplitude variation is a little more than 1%. Another way of viewing this is to examine what we refer to as the "column mass." This is defined by integrating the radial density distribution at a given angle over a spherical volume element; i.e., it is the interior mass distribution the model would have if this radial distribution were spherically symmetric. We show this column mass for three angles versus radial zone number in Figure 6, where it is evident that there is little difference in the mass distribution interior to approximately 5 $M_\odot$. Closer to the model surface there is more mass concentrated in the direction toward the companion, and the column mass monotonically decreases, going away from this direction.

One interesting feature related to the shape of the surface is the rate of change in that shape as the time of RLOF is approached. We compare the expansion rate of the surface in the direction of the companion for the largest separation model with the surface expansion of a spherical model in Figure 7. Clearly, the primary surface in the direction of the secondary is expanding at a much larger rate, one that is fairly close to the expansion experienced in the early phases of hydrogen shell burning. The expansion rate increases yet faster as RLOF is approached, as is evidenced in
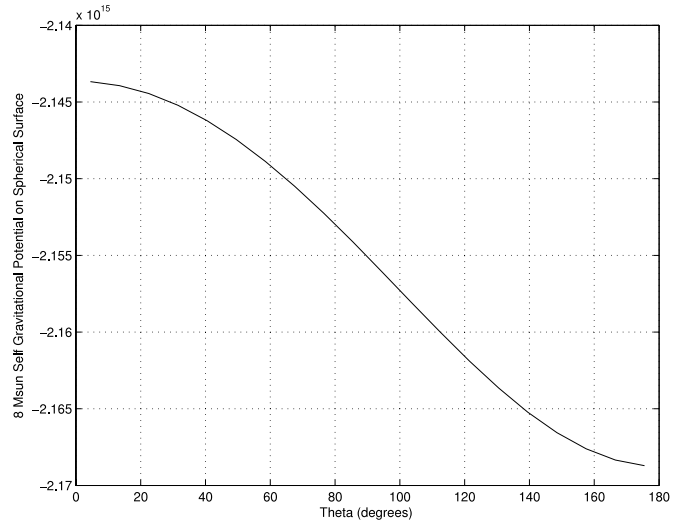

Fig. 5.—Plot of the self-gravitational potential of the 8 $M_\odot$ primary on a spherical surface just exterior to the largest radius of the model vs. the spherical polar coordinate θ. This is for the model very close to RLOF presented in Fig. 4. Note that the self-gravity on this spherical surface varies by about 1% over the surface and is largest in amplitude in the direction toward the secondary.

Figure 8. Here we illustrate the expansion rate of the surface of the primary in the direction of the secondary in the intermediate separation case. The expansion rate is sufficiently rapid, so that it is possible that the stellar surface does not remain an equipotential during this phase, although our calculations assume that it does. This rapid expansion of the surface may also affect the rate of transfer from the primary to the rest of the system, at least near the start of mass transfer.

Another interesting feature is the distribution of the luminosity on the stellar surface. The surfaces of constant temperature
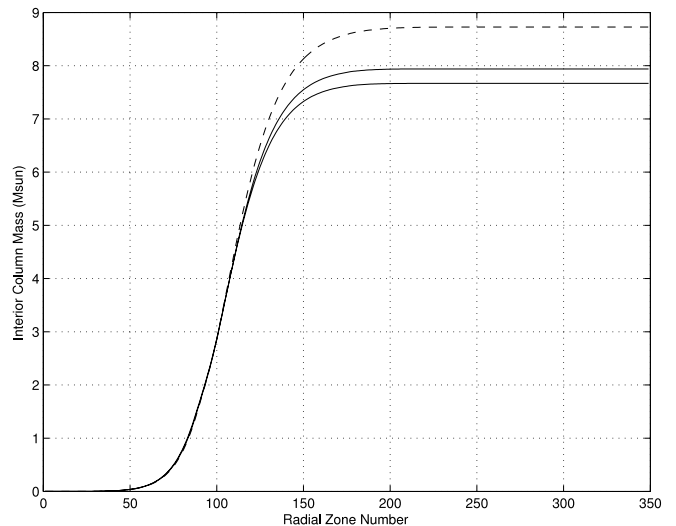

Fig. 6.—Interior column mass vs. radial zone number in the direction away from the secondary (*lower solid curve*), perpendicular to the line joining the centers of the primary and secondary (*upper solid curve*) and in the direction toward the secondary (*dashed curve*). The interior column mass is calculated by taking the radial density distribution at a given angle and calculating the interior mass as if this density distribution were spherically symmetric. This presentation is for the intermediate separation model just before RLOF shown in the previous two figures. The implication is that the mass of the primary has been slightly redistributed by the presence of the secondary to be larger in the direction of the secondary, but only outside the core of the primary. This picture is consistent with the properties of the interior parts of the star, which control the evolution being only very slightly affected by the presence of the secondary.
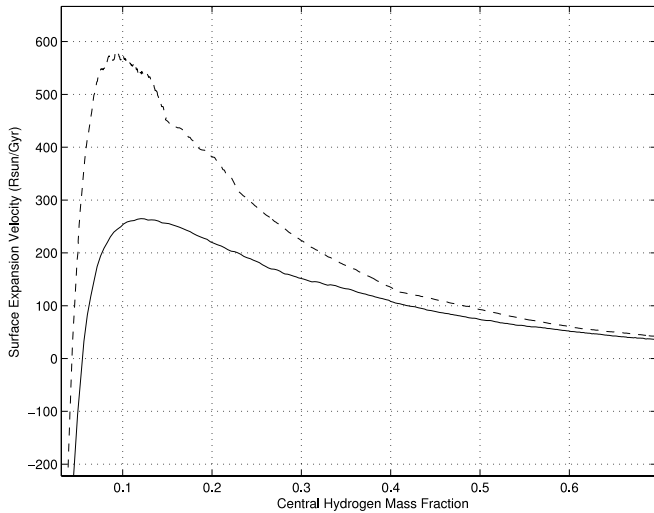
Fig. 7.—Expansion velocity of the surface radius as a function of the central hydrogen-mass fraction. The velocity for a spherical model is given by the solid curve, while the expansion velocity for the surface radius in the direction of the secondary for the primary binary component is given by the dashed curve. The model is the binary with the largest separation. The expansion of the primary accelerates in this direction as RLOF is approached. This model gets close to RLOF before the end of core hydrogen burning, but then moves away from it during the global gravitational contraction phase and eventually overflows the Roche lobe early in hydrogen shell burning.

Fig. 9.—Product of the area of a spherical surface and the radial component of the radiative flux as a function of spherical polar coordinate θ. The solid curve is at a radius a little more than halfway from the center to the surface in the direction of the binary companion. The dashed curve is at the model surface. The radiation flow in the regions between those given by the two curves is away from the line between the centers of the two binary components, as one would expect from the shape of the equipotential surfaces (see Fig. 3). Note that any radiation of the secondary onto the primary has been neglected.

are all extended in the direction of the secondary, so that the direction of radiative diffusion is away from the line between the centers of the two components. Thus, the radial flux drops significantly as one approaches the surface from the interior in that direction. The radial flux drops in the opposite direction for the same reason, but to a much smaller extent. This can be seen in Figure 9, a plot of the local "luminosity," defined to be the area of a spherical surface multiplied by the local radial flux, as a function of θ. We present this luminosity at a radial distance about halfway from the model center to the surface in the direction toward the companion and at the surface. The trend mentioned is present at the deeper location but is quite pronounced at the

surface. The small-scale variations in the surface luminosity are produced by the surface changing its radial zone number on this particular time step. The total luminosity emitted through both surfaces is nearly the same, with the small difference produced by the expansion of the outer layers of the model.

The enlarged surface area produced by the elongation of the model toward the companion has the effect of reducing the average effective temperature, as seen in the evolutionary tracks for a spherical model and the model with the largest separation in Figure 10. This is somewhat illusory, however, for it ignores both the shine of the companion of the secondary onto the surface of the primary and the fact that the observed effective temperature
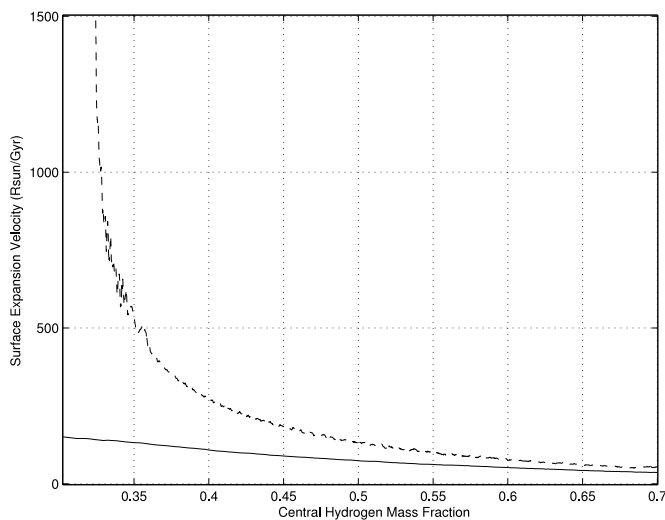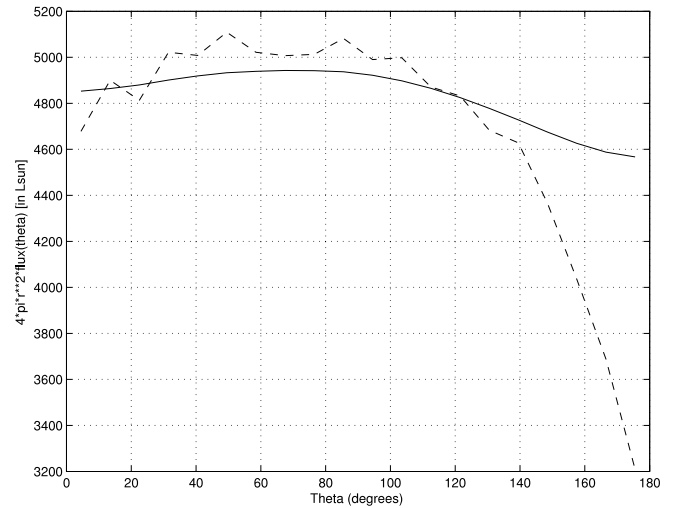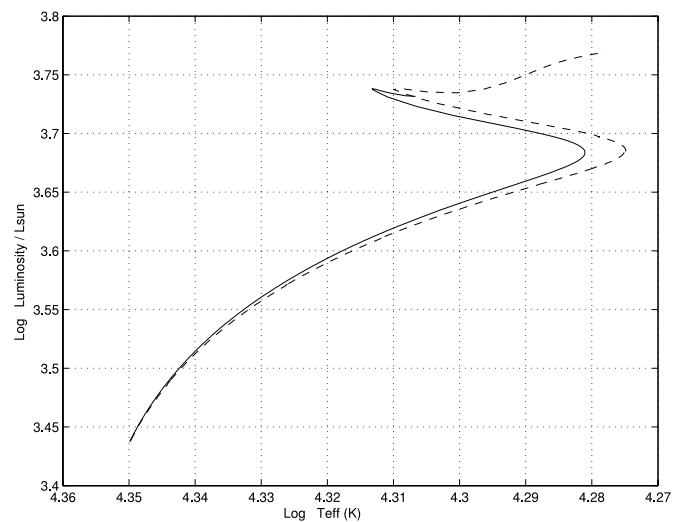

Fig. 8.—Expansion velocity of the surface radius as a function of central hydrogen-mass fraction. The solid curve is for a single-star model, and the dashed curve is for the intermediate separation case. RLOF is expected to occur shortly after the last model shown in the dashed curve. Because the timescale during this end phase becomes very short, it may be possible that the surface is not an equipotential in this latter phase.

Fig. 10.—H-R diagram of the evolution of a single star (solid curve) and of the primary member of the binary system with the largest separation (dashed curve). The two models have the same luminosity history, as one would expect from the nearly identical deep interior structures, but the average effective temperature of the binary member is less, as one might anticipate from Fig. 9. The actual effective temperature one would observe would depend on the orientation of the observer to the binary system.

now becomes a function of the location of the observer with respect to the system geometry.

Throughout this work we have assumed that the secondary may be treated by a point-source potential. It is of some interest to see how significant this assumption is. Therefore we calculated the ZAMS model of the secondary assuming the primary was the point-source companion. This is not completely self-consistent, but it should be adequate to determine some level of credibility for the assumption. We find that the self-gravity of the 5 $M_\odot$ ZAMS model with the 8 $M_\odot$ companion on a spherical surface just exterior to the largest surface radius varies by about 0.6% on that surface.

4. DISCUSSION AND CONCLUSIONS

We have performed two-dimensional stellar evolution sequences of the primary member of a binary system. These sequences were carried through core hydrogen burning up to the time of Roche lobe overflow (RLOF). The interior stellar evolution characteristics were altered from the single-star evolution only on the fraction of a percent level even for the smallest separations. The mass of the convective core as a function of time is also unchanged, although the convective core boundary is no longer a completely spherical surface. Thus, the approximation that the interior structure and evolution is the same as that for a single star appears to be quite good throughout this phase. This can probably be interpreted as being adequate for any stars that are not compact objects, because the smallest separation case was about as small as we could make it on the ZAMS for these two masses. The differences in structure become noticeable at about one-quarter of the radius (equivalent to about an interior mass of 5 $M_\odot$) for the model just prior to RLOF.

The surface is reasonably well approximated by the Roche surface until very close to the beginning of RLOF. As RLOF is approached, the contour lines in the direction of the secondary become very sensitively dependent on the value of the equipotential, and the variations between the Roche potential and the equipotential determined from the models reflect this. It is also true that the timescale for the surface change becomes very short as RLOF is approached, raising the possibility that the assumption that the surface is an equipotential is not valid. It is difficult to identify any consequence of this from the standpoint of the evolution calculations, but it may play a role in the details of the mass transfer within the system.

One important assumption we make in the calculations is that we neglect the radiation from the secondary component, and this radiation could make a considerable difference to the effective temperature and observed surface flux of the primary star, particularly in the direction of the secondary. We can estimate the "true" effective temperature of the primary star by calculating the effective temperature at the surface of the primary using the secondary's luminosity and $L_S = 4\pi\sigma T_{\rm eff}^4 R_D^2$, where L_S is the ZAMS luminosity of the 5 $M_\odot$ model determined by the two-dimensional evolution code, σ is the Stefan-Boltzmann constant, R_D is the distance from the center of the secondary to the surface of the primary, and $T_{\rm eff}$ is the effective temperature. If we take the $a = 14$ $R_\odot$ case as a representative example and the radius of the primary just before RLOF, which is 7.114 $R_\odot$, then $R_D = 6.886$ $R_\odot$ (where the ZAMS radius of the 5 $M_\odot$ two-dimensional model is 2.785 $R_\odot$). Using $L_S = 529$ $L_\odot$, we find that the effective temperature at the surface of the primary using the secondary's luminosity to be 10,561 K. At the angular zone closest to the secondary, the effective temperature of the primary just before RLOF was determined to be 13,476 K, which is 27% hotter than the effective temperature calculated using the luminosity of the secondary model.

We have also calculated the effective temperature at the surface of the primary using the secondary's luminosity just after the ZAMS. This effective temperature was found to be about 2.3 times less than the effective temperature of the primary calculated by the two-dimensional evolution code. The implication of this result for the models near RLOF is that the surface flux of the primary, for example, as shown in Figure 9, should clearly be higher at the angular zones closest to the companion. This also means that the observed dip in the flux is not completely real, and indeed, the effective temperature of the primary closest to the companion should be substantially hotter than what we have calculated it to be using the two-dimensional stellar evolution code. What effect the secondary's radiation has on the interior properties of the 8 $M_\odot$ primary is yet to be determined, and we leave that for future work. We do note that this effect will mostly be important when the primary is rapidly approaching RLOF, and the evolution of the system at this stage is quick enough, so that the radiation from the secondary should not alter our overall conclusions.

REFERENCES

Deupree, R. G. 1990, ApJ, 357, 175
———. 1995, ApJ, 439, 357
Domiciano de Souza, A., Kervella, P., Jankov, S., Abe, L., Vakili, F., di Folco, E., & Paresce, F. 2003, A&A, 407, L47
Fowler, W. A., Caughlan, G. R., & Zimmerman, B. A. 1967, ARA&A, 5, 525
Henyey, L. G., Forbes, J. E., & Gould, N. L. 1964, ApJ, 139, 306
Iben, I., Jr., & Tutukov, A. V. 1996, ApJS, 105, 145
Iglesias, C. A., & Rogers, F. J. 1996, ApJ, 464, 943
Jackson, S., MacGregor, K. B., & Skumanich, A. 2004, ApJ, 606, 1196
Kippenhahn, R., & Weigert, A. 1967, Z. Astrophys., 65, 251
Li, L., Han, Z., & Zhang, F. 2004, MNRAS, 351, 137
Lovekin, C. A., Deupree, R. G., & Short, C. I. 2004, ApJ, submitted
McClintock, J. E., Garcia, M. R., Caldwell, N., Falco, E. E., Garnavich, P. M., & Zhao, P. 2001, ApJ, 551, L147
Nelson, C. A., & Eggleton, P. P. 2001, ApJ, 552, 664

Paczynski, B. 1966, Acta Astron., 16, 97
———. 1967, Acta Astron., 17, 1
———. 1971, ARA&A, 9, 183
Paczynski, B., & Ziólkowski, J. 1967, Acta Astron., 17, 7
Phinney, E. S., & Kulkarni, S. R. 1994, ARA&A, 32, 591
Podsiadlowski, P., Langer, N., Poelarends, A. J. T., Rappaport, S., Heger, A., & Pfahl, E. 2004, ApJ, 612, 1044
Podsiadlowski, P., Rappaport, S., & Pfahl, E. D. 2002, ApJ, 565, 1107
Regős, E., Bailey, V. C., & Mardling, R. 2005, MNRAS, 358, 544
Rogers, F. J., Swenson, F. J., & Iglesias, C. A. 1996, ApJ, 456, 902
Thielemann, F.-K., Brachwitz, F., Höflich, P., Martinez-Pinedo, G., & Nomoto, K. 2004, NewA Rev., 48, 605
Verbunt, F. 1993, ARA&A, 31, 93
Wheatley, P. J., Mukai, K., & de Martino, D. 2003, MNRAS, 346, 855
Yoon, S.-C., & Langer, N. 2004, A&A, 419, 645